Remote Sensing of Environment 125 (2012) 49–63

Contents lists available at SciVerse ScienceDirect

Remote Sensing of Environment

journal homepage: www.elsevier.com/locate/rse

A new time series vegetation–water index of phenological–hydrological trait across species and functional types for Poyang Lake wetland ecosystem

Lin Wang [a,b,c], Iryna Dronova [d], Peng Gong [b,d,e,*], Wenbo Yang [a], Yingren Li [a], Qing Liu [a]

[a] Resources and Eco-environmental Research Center, Chinese Academy of Fishery Science, Beijing 100141, China
[b] State Key Laboratory of Remote Sensing Science, jointly sponsored by the Institute of Remote Sensing Applications of Chinese Academy of Sciences and Beijing Normal University, Beijing 100101, China
[c] Poyang Lake Ecological Research Station for Environment and Health, Duchang 332600, China
[d] Department of Environmental Science, Policy and Management, Division of Ecosystem Science, University of California, Berkeley, CA 94720–3114, USA
[e] Ministry of Education Key Laboratory for Earth System Modeling, Center for Earth System Science, Tsinghua University, Beijing, 100084, China

ARTICLE INFO

Article history:
Received 11 November 2011
Received in revised form 3 July 2012
Accepted 11 July 2012
Available online 3 August 2012

Keywords:
Wetland
Remote sensing
Plant Functional Types (PFTs)
Trait
Classification
Phenology
Submersion time
Multitemporal
Beijing-1 microsatellite
Poyang Lake
Support vector machines (SVM)

ABSTRACT

Despite the long history of vegetation mapping with remote sensing, challenges remain in effectively linking remote sensing observations with plant traits and environmental disturbance across species and functional types. This study proposes a classification of aquatic and wetland vegetation plant functional types (PFTs) using time series remotely sensed data applicable to wetland ecosystems with large annual water level changes like Poyang Lake, the largest freshwater lake–wetland of China. We first developed the aquatic and wetland PFT classification scheme which included perennial C_4 grasses, perennial C_3 reed, C_3 (sedges and taller forbs), short C_3 forbs, floating aquatic macrophytes, and submerged aquatic macrophytes. Using this scheme, time series normalized difference vegetation index (time series NDVI) images and time series vegetation–water index (time series VWI) images extracted from 32-m spatial resolution Beijing-1 microsatellite data were applied to perform two PFT classifications with a support vector machine (SVM) algorithm. We found that the time series NDVI-based SVM classification method mapped aquatic and wetland PFT distribution with an overall accuracy of 81.3%. However, when the information on water level fluctuation was combined with time series NDVI into a new time series index (referred to as time series VWI), the overall accuracy increased to 90.4%. Results suggest that time series VWI has a stronger capability in distinguishing wetland PFTs with different submersion times and flood tolerances than time series NDVI, and thus may be considered as a key input dataset for future PFT classifications in seasonally dynamic wetlands.

1. Introduction

Both aquatic vegetation and water fluctuations play important roles in ecosystem processes and functioning of seasonally or intermittently inundated wetlands (Johnston & Barson, 1993; Junk, 1997; Marion & Paillison, 2003). The interactions between the flooding regime, local topography and ecophysiological performance of vegetation may result in diversification of plant traits and functional attributes along the inundation gradients (Boutin & Keddy, 1993). At the landscape level, this variation is often expressed as belt-shaped plant type "zonation" around the water body (Lenssen et al., 1999). "Zones" formed by vegetation groups with different tolerances to flooding and submersion times may represent a convenient framework for studying wetland surface and associated ecosystem function. However, selection of vegetation categories that can adequately represent variation in plant function along the moisture gradients and effectively simplify ecological complexity for ecosystem monitoring is still challenging in heterogeneous and dynamic wetland landscapes.

Identification of the natural patterns following environmental changes by organizing groups of plant species into functional groups have long been adopted by ecologists (Boutin & Keddy, 1993; Cowardin et al., 1979; Hutchinson, 1975; Keddy, 1992; McGill et al., 2006; Menges & Waller, 1983; Smith et al., 1997). Recently, the concept of Plant Functional Type (PFT) has received greater attention in biogeographic and ecological modeling efforts which require ecologically meaningful generalizations of vegetative cover (e.g., Bonan et al., 2002; Chapin et al., 1997; Díaz & Cabido, 1997; Epstein et al., 2001; Smith et al., 1997) to simulate and forecast regional and global landscape changes. Furthermore, ecological research initiatives have started integrating plant functional classifications with biogeochemical models (Cao & Woodward, 1998; Li & Frolking, 1992; Melillo et al.,

* Corresponding author at: State Key Laboratory of Remote Sensing Science, jointly sponsored by the Institute of Remote Sensing Applications of Chinese Academy of Sciences and Beijing Normal University, Beijing 100101, China. Tel.: +86 10 62788023.
E-mail address: penggong@tsinghua.edu.cn (P. Gong).

0034-4257/$ – see front matter © 2012 Elsevier Inc. All rights reserved.
doi:10.1016/j.rse.2012.07.003

1993) for predicting ecosystem response to anthropogenic pressures and climate change.

Very recently, the concept of 'optical type' was proposed (Ustin & Gamon, 2010), which emphasizes the linkages among plant functional traits (e.g. morphological, physiological and phenological features affecting biomass, productivity or ability to withstand disturbances) and spectral reflectance of vegetation that can be detected with remote sensing technologies. Various previous studies on PFT mapping with coarse- and medium-resolution remotely sensed data (Bonan et al., 2002; Strahler et al., 1999; Sun et al., 2008) have been conducted mainly in terrestrial ecosystems. In those studies PFT classification schemes focused on upland vegetation, while wetlands and water were often integrated and treated as a single class. However, efforts on mapping wetland or aquatic PFTs using multispectral medium-resolution remote sensing data are still rare, and there have been little attempt to combine in situ assessed ecological characteristics of vegetation with remotely sensed multi-temporal plant signatures to characterize PFTs in seasonally dynamic wetlands.

In this study, we proposed new time series indicators extracted from the images of the recently launched Beijing-1 microsatellite to conduct the PFT classification for Poyang Lake, the largest freshwater lake–wetland ecosystem in China (Fig. 1) characterized by considerable inter-annual water fluctuations due to hydrological and climate cycles. As one of the few remaining dam–free water systems along Yangtze River, Poyang Lake is a critically important wetland conservation site which provides winter habitat for large numbers of wild waterbirds including many endangered species (Gong et al., 2010; Ji et al., 2007; Niu et al., 2009, 2011; Zheng et al., 2012). However, it faces potentially serious yet poorly understood threats from climate and land use changes, hydrological effects of the massive Three Gorges Dam upstream Yangtze, and a controversial proposal of the new local dam for maintaining adequate water supply in flood-free seasons (Finlayson et al., 2010; Li, 2009). Many scientists and environmentalists have argued that this proposed water-control structure would have a significant negative impact on wintering waterbirds due to high risk of losing most of the suitable shallow-water habitats (Barzen, 2008, 2009; Finlayson et al., 2010; Li, 2009). However, no studies to date have adequately assessed seasonal distributions and dynamics of Poyang Lake wetland vegetation types that shape avian habitat features and food resources. This creates an urgent need to map the spatial distribution of the aquatic vegetation at the PFT level to facilitate modeling of Poyang Lake wetland environment and waterbird habitat under scenarios of the future climate change and anthropogenic alterations of this region.

In this study, we explored new approaches to link the observations from multi-spectral medium-resolution remote sensing data with functional traits of wetland vegetation and flood-driven local environmental disturbance, to produce the PFT map of annually dominant Poyang Lake vegetation. PFTs were classified with the support vector machines (SVM) algorithm, which is suitable for wetland analyses for its ability to achieve high classification accuracy even with small training sample sizes (Foody & Mathur, 2004; Tax & Duin, 2004). Our specific objectives were: 1) to propose a preliminary freshwater lake–wetland aquatic PFT classification scheme derived via a two-step hierarchical cluster analysis of 51 plant species and relevant traits, 2) to compare the success of PFT discrimination between two time series remote sensing index images emphasizing vegetation greenness versus combined greenness and wetness, and 3) using Poyang Lake as an example of seasonally inundated wetland, to map aquatic PFTs with SVM from the time series index images and

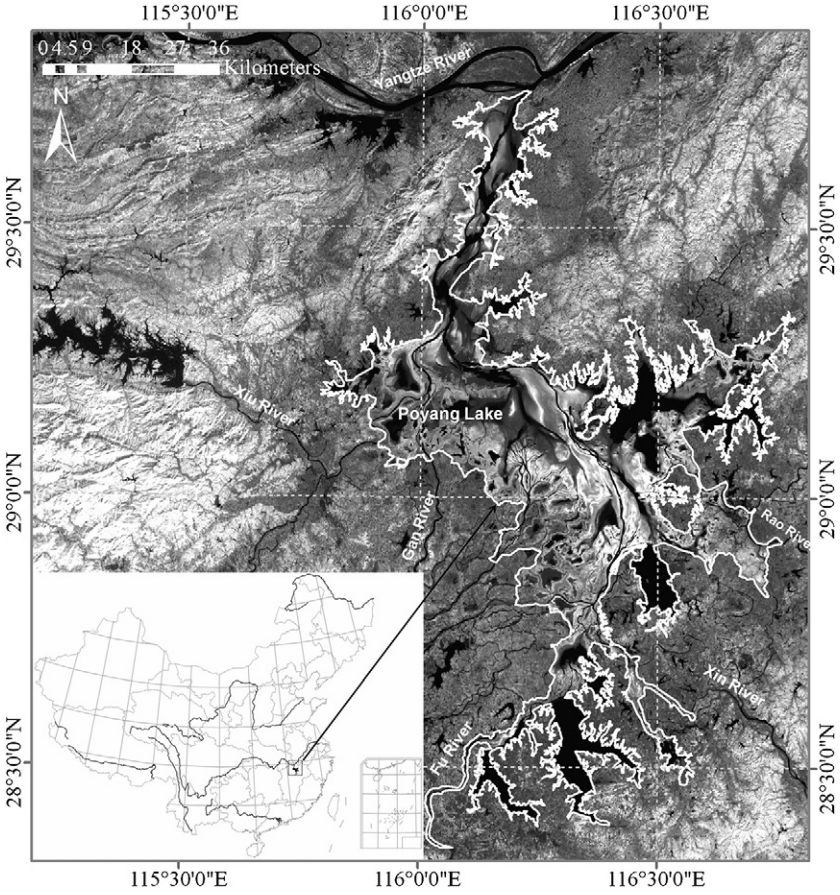

Fig. 1. Spatial location of Poyang Lake, Jiangxi Province, People's Republic of China.

to investigate the association among PFT distributions and seasonal flood-driven disturbance pattern.

2. Materials and methods

2.1. Study site

Poyang Lake is located between 28°22′–29°45′N and 115°47′–116°45′ E. It lies in the northern part of Jiangxi Province, China, at the southern bank of the lower reach of the Yangtze River (Fig. 1). It is a basin marsh wetland (Warner & Rubec, 1997) with 1200-km long lakeshore and covers a water area of 3569 km^2 (when the water level at Hukou station is 17.9 m, Wu Song Elevation), which varies greatly within a year following fluctuation of its water level. The most common wetland components include: non-persistent seasonal wetland with tall perennial emergent vegetation of the river banks and low-lying catchments and medium to short perennial lakeshore vegetation; aquatic beds with submerged or floating-leaved rooted macrophytes; and seasonally exposed lake bottomland with mudflats, sand and shallow water (Cowardin et al., 1979; Liu & Ye, 2000).

In this study we focused on Poyang Lake PFTs and wetland dynamics from April 2007 to May 2008 covering one winter growing season and one summer flood period. According to the monthly mean of the daily water level data measured at Duchang Hydrological Station (Qi et al., 2009) between Jan 1, 2007 and December 31, 2008 (Fig. 2), the temporal change patterns were almost consistent between 2007 and 2008 years, especially during water infill, high water level and water subsiding periods. This indicates that Poyang Lake should have experienced similar vegetation change patterns according to water level changes in both 2007 and 2008. No extreme drought or flood events had been reported or indicated by hydrological data during those two years (Fig. 2).

2.2. Remote sensing data acquisition and pre-processing

Considering the large size of Poyang Lake and common cloudiness which limit frequent acquisition of high-resolution images, we chose 10 scenes from April 2007 to May 2008 (Table 1) of Beijing-1 32-m multispectral microsatellite sensor (Surrey Satellite Technology Ltd) for their moderate spatial and spectral resolution (Wright & Gallant, 2007), wide 600 km swath and 5-day revisit interval. This multispectral sensor has three bands covering the green (0.52–0.62 μm), red (0.63–0.69 μm) and near infrared (0.76–0.9 μm) spectral regions suitable for vegetation analyses. Because this sensor does not have a calibration system on board, we used only Digital Numbers (DNs), and not ground-level reflectance, in the analysis. Prior to the time series analysis, we radiometrically calibrated (Gong et al., 1994) all other images to the image of Feb 16, 2008 with the least atmospheric noise using pseudo-invariant targets selected among temporally stable features, specifically: seven bright targets such as large concrete squares, white sand on high topographic features in the central part of the lake and seven dark targets such as no-change water reservoirs in cities. Next, radiometrically calibrated images were georeferenced to the 10 Dec 1999 Landsat TM scene using the ENVI v.4.3 software (Research System Inc.). We did not conduct topographic correction because the study area is flat. Before the classification we isolated the main lake–wetland area from its surroundings by a mask developed from images of the highest summer flood extent.

Table 1
The image data used in this study. All are level 1A data from the data provider.

Date	Hydrological period	$y = ax + b/r^2$	GCPs	Cloud coverage/ if over Poyang Lake	RMSE
19/04/2007	Infilling	y = 0.98x + 16.36/0.84	21	0	0.4812
06/05/2007	Infilling	y = 0.91x + 19.49/0.66	315	<2%/NO	0.9278
26/07/2007	High water level	y = 1.53x − 62.28/0.85	28	0	0.4273
16/08/2007	High water level	y = 0.87x + 14.46/0.80	26	<2%/NO	0.4942
17/10/2007	Draw-off	y = 1.21x − 4.45/0.94	25	<2%/YES	0.4953
30/11/2007	Draw-off	y = 1.44x − 44.28/0.96	24	0	0.4114
01/01/2008	Low water level	y = 1.28x − 29.12/0.97	28	0	0.8993
16/02/2008	Low water level	y = x/1.00	28	0	0.4492
02/03/2008	Infilling	y = 1.63x − 49.03/0.91	25	0	0.3448
12/05/2008	Infilling	y = 1.87x − 90.25/0.87	32	<2%/YES	0.4547

Note: we used 10 scenes of Beijing-1 multispectral images with 32 m spatial resolution. $y = ax + b$ means the empirical linear model for relative radiance calibration of each of images to Beijing-1 Feb 16, 2008 scene, r stand for the correlation coefficient which gives the quality of a least squares fitting to Feb 16, 2008 scene. GCPs and RMSEs stand for the number of ground control points used for georegistration and the root mean square errors from georegistration for each scene. A Landsat TM data (30 m resolution) acquired on 10 Dec 1999 was used as a base to which all other Beijing-1 images were registered. The image acquired on 06/05/2007 produced an abnormal geometrical distortion, so we used a lot more ground control points to make sure that the resultant RMSE was less than 1.

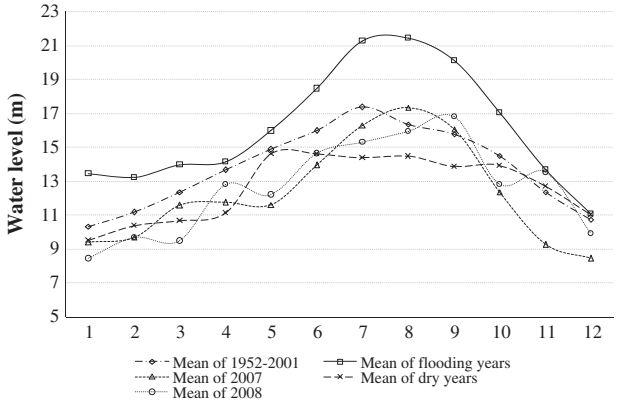

Fig. 2. Comparison of monthly mean of water level between 2007, 2008, 1952–2001, historical flood years (1954 and 1998) and dry years (1963 and 1972).

2.3. Field data collection and design of the PFT classification scheme

Field surveys of vegetation were conducted in April 2006, March 2007, December 2007–Jan 2008, April–May 2008, November 2008, and May 2009. We also referred to the published analyses of Poyang Lake vegetation which estimated the composition and abundance of plant species at the small plot level (Barzen, 2008, 2009; Li & Liu, 2002; Liu & Ye, 2000; Michishita et al., 2008; Wang, 2004; Wu, 2008; Zhang, 1988; Zheng, 2009). Based on this information, 51 commonly dominant plant species were selected to represent wetland habitats and functional groups along the inundation gradients across the Poyang Lake lake–wetland ecosystem. Plant species' traits were measured at the individual level, while community composition was assessed from 1 × 1 m plots sampled along transects that were laid out perpendicular to the water margin. Overall, field data combined from different sampling events covered 20 transects of 500–2000 m in length depending on field access from the roads or by boat and presence or absence of flooding. Along these transects the frequency of sampling was at least 50–100 m, but more frequent sampling was

performed near the water boundaries where different vegetation types occurred in narrow zones. We also recorded geographic coordinates of the plot center, additional landscape characteristics and vegetation composition homogeneity for the area of 60×60 m and greater around the plots. Some of the revisited plots were observed several times to verify that they contained the same dominant aquatic vegetation communities during the 2007–2008 low water periods.

To develop the Poyang Lake PFT classification scheme for subsequent PFT mapping from remote sensing images, we used 10 key vegetation traits and 4 characteristics of the sample plots and surrounding areas (Table 2). We focused on 1) traits describing photosynthesis pathway and carbon storage potential, inundation tolerance, morphology and phenology, and 2) characteristics related to waterbird foraging preferences, plot-level plant percent cover, and homogeneity of landscape composition around the sample plots.

The PFT classification scheme was generated using a two-step hierarchical cluster analysis of 51 species by their traits (Table 2) with SPSS statistical software. In the first step, traits 1–6 and characteristic 1 of the sample plots (Table 2) were used to discriminate between major PFTs with squared Euclidean distance coefficients. In the second step, traits 7–10 were further used to select more specific minor PFTs with Pearson correlation coefficients (Wilksinson, 1984). Once the dendrogram of PFTs was generated, Fisher's linear discriminant functions were applied (Table 2) to determine which traits contributed most strongly to statistical differences among the resulting PFT categories (Norušis, 2008). Characteristics 2 to 4 (Table 2) were used in training and test sample selection in subsequent remote sensing image classifications.

2.4. Discriminating the aquatic PFTs using remotely sensed data

In order to assess the benefits of Beijing-1 microsatellite sensor imagery for classifying Poyang Lake wetland PFTs, we compared two multi-date remote sensing indices: 1) time series normalized difference vegetation index (time series NDVI) images which highlighted differences in PFT greenness potentially related to functional group composition, phenology, biomass, foliar pigment content and photosynthetic light-use efficiency; and 2) a new time series vegetation–water index (time series VWI) images which emphasized differences in flooding tolerances among separate functional groups.

The first set of time series index images was developed based on previous reports of single-date NDVI as a useful general indicator of community type, plant biomass, foliar pigment composition and

Table 2
Traits recorded on the 51 representative species and the characteristics of the plot over Poyang Lake wetland area. At least 9–10 randomly chosen, healthy looking individual plants sampled along an elevation gradient from across the Poyang Lake lake–wetland ecosystem were considered for traits measured in the field or collected in the previous studies. The originally categorical, continuous and binary variables were all scaled into categorical for this analysis.

Trait	Description	Description of variables in analysis
Traits recorded on the 51 representative species		
1-Photosynthesis pathway	Photosynthetic metabolism, on the basis of literature[1] and leaf anatomy observation	Using in dendrogram acquisition $C_4=1$; $C_3=2$
2-Carbohydrate storage	Capacity to store carbohydrate than can be broken down and allocated to new growth (thickened roots and stems, bulbs, rhizomes)[2]	Using in dendrogram acquisition no specialized storage organs = 0; slightly storage organs = 1; strong storage organs = 2
3-Carbon immobilization	Capacity to invest C in support tissue (xylem and bark), in compounds that cannot be broken down to be used in further biosyhthesis[2]	Using in dendrogram acquisition herbaceous monocots = 1; Herbaceous dicots = 2
4-Life span	The period to complete its life cycle of the non-woody plant, based on literatured[3] and field observation	Using in dendrogram acquisition perennials = 1; annual or biennial = 2
5-Life-forms	the relationship to the height of the water table, based on literatured[3] and field observation	Using in dendrogram acquisition hygrophyte = 1; emergent = 2; floating = 3; submerged = 4
6-Ramification	Degree of ramification at the base of the plant[4]	Using in dendrogram acquisition no evident divided = 0; evident divided = 1;
7-Reproductive phenology	Seasonality of maximum production of flowers and fruits, based on literature[3] and field observation	Using in dendrogram acquisition no evident peak = 1; winter, autumn, early spring = 2; spring, late spring, spring–summer, late summer–early autumn = 3; late spring–summer, summer = 4
8-Percentage flowering of the year	Percentage flowering of the year, based on literature[3] and field observation	Using in dendrogram acquisition 0 –≤0.25% = 1; >0.25–<0.50 = 2; 0.50–≤1 = 3
9-Maximum height	Maximum height of species above the ground with percent cover ≥20%, based on field observation	Using in dendrogram acquisition 0 –≤10 cm = 1; >10–<50 = 2; 50–<100 = 3; ≥100 = 4
10-Leaf area	Leaf length×width of per leaves (cm^2)[5], based on field observation	Using in dendrogram acquisition aphyllous = 0; >0–<10 cm^2 = 1; 10–<50 = 2; 50– ≤100 = 3; >100 = 4
Characteristics of or around the sample plot		
1-Habitat types	Supporting distinct foraging guilds by birds, on the basis of literature[6]	Using in dendrogram acquisition no specified foraging guild = 1; foraging guild include Greater White-fronted Geese, Lesser WhitefrontedGeese, Greylag Geese (*Anseranser*), Bean Geese (*A. fabalis*), and often Swan Geese = 2; foraging guild include mallard, gadwall, spot-billed duck andcommon teal. = 3; represented by Siberian Cranes, Hooded Cranes(*Grusmonacha*), White-naped Cranes, Eurasian Cranes (*Grusgrus*) and Swan Geese = 4
2-Percent cover	Estimated percent cover for each species and non-vegetated cover type (if present) such as water, sand, mudflat, based on field observation;	Connecting the above known ground traits to the imagery
3-Landscape characteristics	Recorded the vegetation landscape characteristics and homogeneity level around the plots more than 60×60 m area (corresponding to 2×2 pixels on Beijing-1 images), based on field observation	Training samples were selected at the image points corresponding to the field sample plots with the ≥80% cover by the species from each PFT and homogeneous landscape composition for 60×60 m or more around them
4-Sampling position	Recorded the geographic coordinates of the plot center, based on field observation	

Description:
[1] Beale et al., 1996; Edwards et al., 2010; Still et al., 2003; Zheng, 2009.
[2] Positively related with sink strength for carbon (Díaz, 1995; Poorter, 1993).
[3] Liu & Ye, 2000; Wang, 2004.
[4] Considered an advantage under severe water stress (Díaz & Cabido, 1997).
[5] Important for energy balance and hydraulic architecture, with smaller leaves generally observed in drier and more exposed conditions (Ackerly & Cornwell, 2007).
[6] Barter et al., 2004, 2006; Barzen, 2008, 2009; Cheng, 1987; Fang et al., 2006; Ji et al., 2007.

Table 3
Summary of characteristics of the main plant functional types (PFTs) produced by two steps hierarchical cluster analyzing of the matrix of 51 species by above 10 traits and 4 characteristics over the Poyang Lake lake–wetland ecosystem (number of species in each PFT included in brackets).

PFTs	Growth form	Vegetative traits
PFT 1–1 (6) Perennial C_4 grasses	Upland dry, water table not greater than 1.7 m below soil surface to 1–2 m above the soil	C_4 pathway; High carbohydrate storage; All species are herbaceous monocots and perennial; Some C-immobilization in xylem and bark; Some high ramified at ground level; No specified foraging guild by birds; Production of flowers and fruits peak: late spring–early summer; Various canopy height above the soil from 20 to 280 cm with average 117.6 cm; Average percentage flowering of the year is 36.2%; Average leaf area of per leaves is 62.4 cm^2
PFT 1–2 (6) Perennial C_3 reed	River banks or low-lying catchments; Water table from 0.5 m below the soil surface to 1–2 m above the soil	C_3 pathway; Moderate to high carbohydrate storage; All species are herbaceous monocots and perennial; No evident ramification; Foraging guild by birds include Greater White-fronted Geese, Lesser White fronted Geese, Greylag Geese (*Anseranser*), Bean Geese (*A. fabalis*), and often Swan Geese; Production of flowers and fruits peak: late spring–summer, summer; Canopy height above the soil from 12 to 270 cm with average 135.3 cm; Average percentage flowering of the year is 32.1%; Average leaf area of per leaves is 57.9 cm^2
PFT 2–1 (9) C_3 (sedges & taller forbs)	Lakeshores/open flat marshland; Water table from 0.5 m below the soil surface to 1–3.5 m above the soil	C_3 pathway; Moderate carbohydrate storage; Short-term C-immobilization in standing dead matter; Various lifespans; Have no or very low ramification at ground level; Foraging guild by birds seems as PFT 1–2; Various production of flowers and fruits peak: winter, autumn, early spring; spring, late spring, spring–summer, late summer–early autumn; Canopy height above the soil from 35 – 140 cm with average 79.9 cm; Average percentage flowering of the year is 25.8%; Average leaf area of per leaves is 37.5 cm^2
PFT 2–2 (17) Short C_3 forbs	Lakeshores/open flat marshland especially the narrow transition zone between the lake and the marshland; Water table from 0.2 m below the soil surface to 1–4 m above the soil	C_3 pathway; Low to moderate carbohydrate storage; Very low to nil C-immobilization in xylem; All species are herbaceous dicots and ramified at ground level; Various lifespans; Foraging guild by birds seems as PFT 1–2; Production of flowers and fruits peak: spring, late spring, spring–summer, late summer–early autumn; Canopy height above the soil from 14 – 59 cm with average 32.3 cm; Average percentage flowering of the year is 34.8%; Average leaf area of per leaves is 13.6 cm^2
PFT 3–1 (5) Floating aquatic macrophytes	Mud-forming floating on the water surface at water height above the soil surface at water depths 0.3–2 m	C_3 pathway; Low to moderate carbohydrate storage; Various lifespans; stem ramified; Foraging guild include mallard, gadwall, spot-billed duck and common teal.; Production of flowers and fruits peak: spring, late spring, spring–summer, late summer–early autumn; Canopy height under water from 145 to 80 cm with average 114.3 cm; Average percentage flowering of the year is 44.8%; Average leaf area of per leaves is 31.3 cm^2
PFT 3–2 (8) Submerged aquatic macrophytes	Under the water at 0.2–3 m water depths	C_3 pathway; Low carbohydrate storage; All perennial; All stem ramified; Foraging guild represented by Siberian Cranes, Hooded Cranes(*Grusmonacha*), White-naped Cranes, Eurasian Cranes (*Grusgrus*) and Swan Geese; Various production of flowers and fruits peak: winter, autumn, early spring; spring, late spring, spring–summer, late summer–early autumn; Canopy height under water from 220 to 100 cm with average 156.4 cm; Average percentage flowering of the year is 38.5%; Average leaf area of per leaves is 13.6 cm^2

photosynthetic performance of aquatic vegetation (Peñuelas et al., 1993). Time series NDVI images were simply stacking the ten single-date NDVI images (Table 1).

The second set of time series index images was developed to combine the information in time series NDVI with image-derived changes in water extent because no detailed and accurate bathymetry data on the bottom of Poyang Lake or the inundated marshland areas were available for our study. Specifically, we proposed a new time series vegetation–water index (time series VWI) which combined the multi-date information on greenness and surface wetness and thus could emphasize differences in hydrological tolerance among vegetation groups of interest. For time series VWI calculation, spatial extents of the water body were first extracted as binary layers from the negative NDVI images of each scene using density-slicing and thresholding approaches (Hui et al., 2008). Simple density-slicing was considered as a suitable technique that could be more easily related to physical parameters of the surface than complex statistical methods (Johnston & Barson, 1993). Next, the annual submersion time index was estimated as the average of the extracted water body layers (Andreoli et al., 2007):

$$Submersion\,Time\,Index(\omega) = \frac{1}{10}\sum_{m=1}^{10}\omega_m, \quad (1)$$

where m is month of the year for water level fluctuation characteristics; ω_m is a water extent layer extracted from Beijing-1 images for month m and $\omega_m \in \{0,1\}$. The submersion time can reflect the dynamics of water depth since lower elevation location should have longer submersion time. Finally, the time series VWI was calculated as the ratio of time series NDVI images to Submersion Time Index (Eq. 2):

$$\text{Time series VWI} = \frac{\text{time series } NDVI}{Submersion\,Time\,Index} \quad (2)$$

The greater the Submersion Time Index is, the smaller the time series VWI would be, implying a wetter surface condition or much bigger flooding disturbance. Next, we assigned representative PFT locations from time series NDVI and time series VWI images to 1) select training and test sample pixels for image classification, 2) to compare the temporal variation in spectral reflectance among different PFTs and 3) to assess the ability of time series NDVI and time series VWI to distinguish among different PFTs. Specifically, we selected all the image pixels which corresponded to field sample plots with ≥80% cover by the species from each PFT and consistent (homogeneous) landscape composition for 60×60 m or more around them. This way selected pixels could be considered representative of their respective PFTs at 32-m image resolution. From the training sample pixels of each PFT (the specific number of training pixels for each class was given in Section 2.5) we then calculated basic descriptive statistics (maximum, minimum, mean and standard deviations (SD)) for time series NDVI, submersion time index and time series VWI. Mean PFT sample values from individual layers within time series NDVI and time series VWI were used to construct the time series curves representing spectral profiles of PFTs across image dates, here referred to as time series NDVI curves and time series VWI curves, respectively. Finally, we conducted pairwise comparisons of PFTs across all dates using one-way ANOVA with Games–Howell post hoc test (Norušis, 2008) in time series NDVI curves and time series VWI curves.

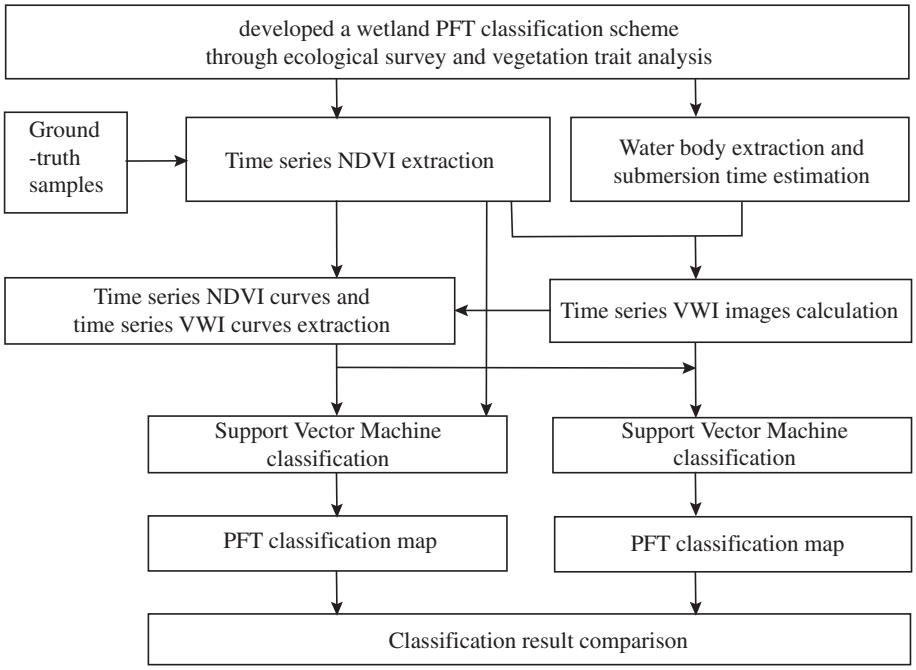

Fig. 3. A flowchart of Plant Functional Type (PFT) classification over Poyang Lake.

2.5. Image classification

We separately classified time series NDVI and time series VWI images into PFTs derived via hierarchical cluster analysis (Fig. 4, Table 3) using the SVM algorithm with the radial basis function (RBF; Hsu et al., 2010; Kavzoglu & Colkesen, 2009) in ENVI 4.8 software. The sample pixels selected as described above were randomly divided into the training set and the test set, 540 sample pixels for each set corresponding to the field-survey plots for PFTs and non-vegetated land cover types (specifically 32, 37, 53, 47, 40, 85, 76, 81, 89 of training and 55, 33, 72, 41, 67, 93, 44, 61, 74 of test sample for C_4 grasses, C_3 reed, C_3 (sedges and taller forbs), short C_3 forbs, floating aquatic macrophytes, submerged aquatic macrophytes, mudflat, water and sand, respectively). We tested multiple values of SVM parameters (C, γ) at a coarser search scale ($C=2^{-1}, 2^{1}, 2^{3}, \ldots, 2^{13}$ and $\gamma=2^{-5}, 2^{-3}, \ldots, 2^{3}$) and further the finer search scale (such as $C=2^{3.2}$, $2^{3.4}, \ldots, 2^{3.6}$), to select the combination which produced the highest cross-validation accuracy of the training set (Hsu et al., 2010; Kavzoglu & Colkesen, 2009). Then we applied the trained algorithm to the test set and estimated the resulting confusion matrices for the 6-class PFT set and non-vegetated cover types. Finally, the overall and class-specific PFT classification accuracies were compared between results from the two input time series index images (Fig. 3).

3. Results

3.1. Dendrogram of plant functional types

The dendrogram resulting from the hierarchical cluster analysis (Fig. 4) shows the assignment of selected plant species into three major PFTs (emergent plants, hygrophilous vegetation and aquatic macrophytes), each containing two minor PFTs (six functional groups total) with the distinct vegetative traits and growth form (Table 3). Fisher's linear discriminant functions of these six minor PFTs showed that their best discriminating traits included life form, reproductive phenology, maximum height, leaf area, and carbohydrate storage (Table 2).

3.2. Discriminating the aquatic PFT using remote sensing data

Assessment of PFT differences in time series NDVI and time series VWI datasets (Fig. 5, showing only PFTs 1–6) highlighted the diverse multi-temporal spectral signatures of these classes. This assessment was based on the 540 training sample pixels selected from field survey data. Perennial C_4 grasses (Fig. 5c), being the least affected by water inundation and disturbed by water for only 1–2 months per year, represented "upland" vegetation phenology with two annual peaks of greenness in April–May and October. Perennial C_3 reeds (Fig. 5c) have only one peak of greenness of April–May. Compared with C_4 grasses, this group had relatively higher NDVI values from May–August because these more hygrophilous reeds can survive during the water infilling period and also maintain high abovewater biomass during the high water level period. In contrast, C_3 (sedges and taller forbs) and short C_3 forbs (Fig. 5e) were completely submerged by the annual water inundation from approximately middle May to the end of September, which resulted in their low NDVI during July–September, despite higher availability of light and warmer temperatures during this period. These two minor PFTs have two greenness peaks per year, April–May and Nov–Jan. Higher November to March NDVI values for C_3 (sedges and taller forbs) compared to other PFTs could reflect relatively higher biomass and density of this PFT during the low water period (Fig. 5a); this result was consistent with our field observations. The NDVI values of the floating aquatic macrophytes (Fig. 5g) in April–May were twice as high as those in October at the time of senescence, also consistent with field observations. For the submerged aquatic macrophytes (Fig. 5g), all the NDVI values except July–August maintained relatively stable level (Table 3). The low July–August index values of the submerged aquatic macrophytes could be attributed to the NIR absorption by water and light scattering from suspended particles. The period from October to May was the most useful for detecting submerged aquatic macrophyte beds because at this time water levels decline and NDVI is more sensitive to presence of plant canopies in shallow waters.

According to time series NDVI curves and time series VWI curves (Fig. 5), the overall seasonal change trends were consistent between each pair of minor PFTs and between time series NDVI versus time

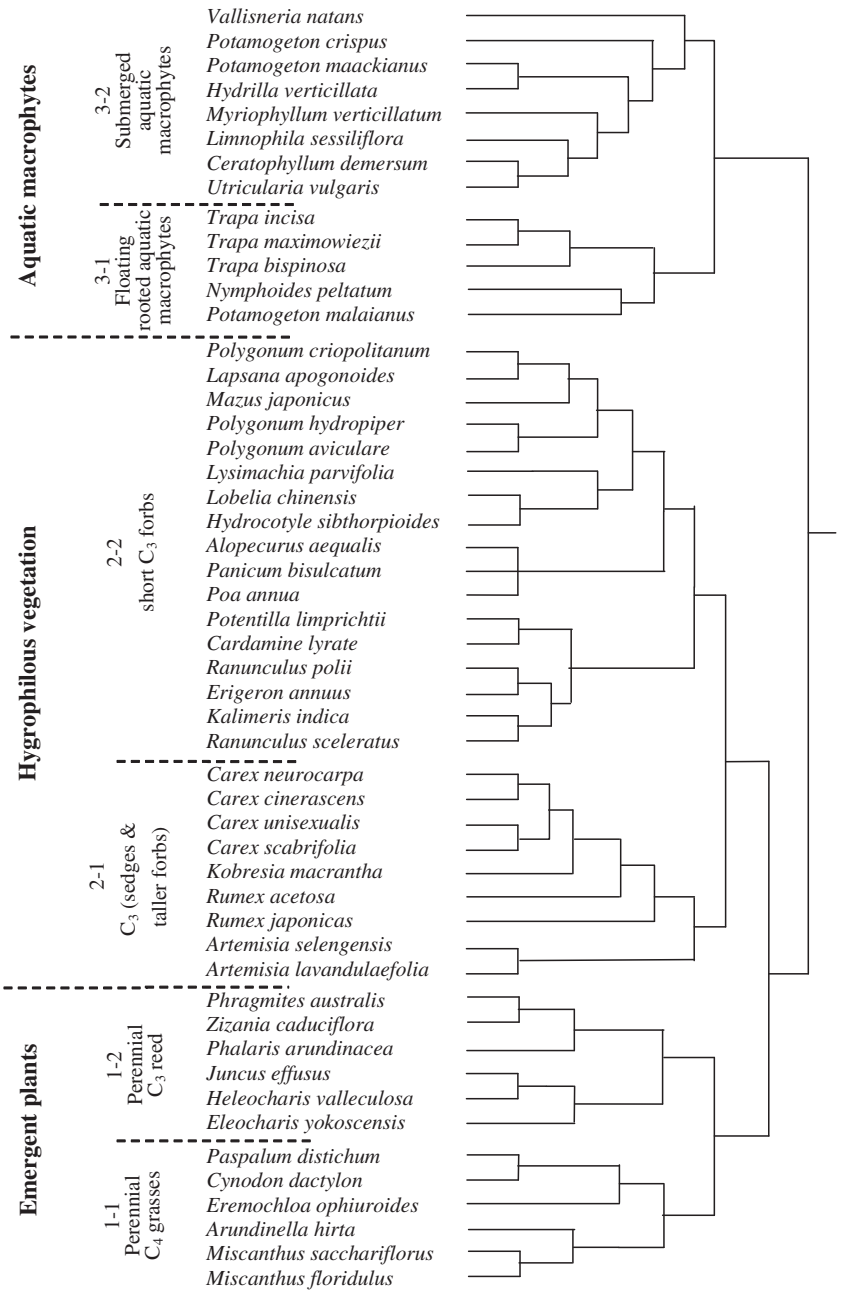

Fig. 4. Dendrogram showing the hierarchical clustering results of 51 lake-wetland plant species. The aquatic macrophytes are shown on the top of this chart, whereas the emergent plants are displayed near the bottom. The names of major and minor PFTs are labeled on the left side.

series VWI images, except for perennial C_3 reed class (Fig. 5c, d). The change trends for the latter PFT were different due to large variation of submersion time among locations representing this PFT during high water level periods.

For three major PFTs, the contrast between emergent plants and hygrophilous vegetation was considerably enhanced in time series VWI curves verses time series NDVI curves (Table 4, with 0.49 of *p-value* in time series NDVI and <0.001 in time series VWI), while the other two pairs of major PFTs had significant difference both in time series NDVI and time series VWI images. For six minor PFTs, there were two important enhancements of class separation in time series VWI compared to time series NDVI. First, the differences between the pairs of fall into one major class, such as C_3 reed vs. C_4 grasses and C_3 (sedges and taller forbs) vs. short C_3 forbs, were improved in time series VWI verses time series NDVI. Second, the pairs of PFTs that may be spatial neighbors had no significant differences from time series NDVI images, but were effective separated from time series VWI images (with *p-value*<0.001, Table 4).

3.3. Image classification

The search for the optimal pairs of the SVM parameters *C* and γ to maximize classification accuracy (Fig. 6) found that kernel width γ had a smaller effect on the performance of RBF than *C*: the γ values in the range of 2^{-1}-2^{-3} produced the same overall accuracy when *C* remains unchanged, consistent with results in Kavzoglu and Colkesen (2009). The best (C, γ) were set to ($2^{3.4}$, 2^{-3}) and ($2^{9.2}$, 2^{-3}) in the classification of the six minor PFT using time series NDVI and time series

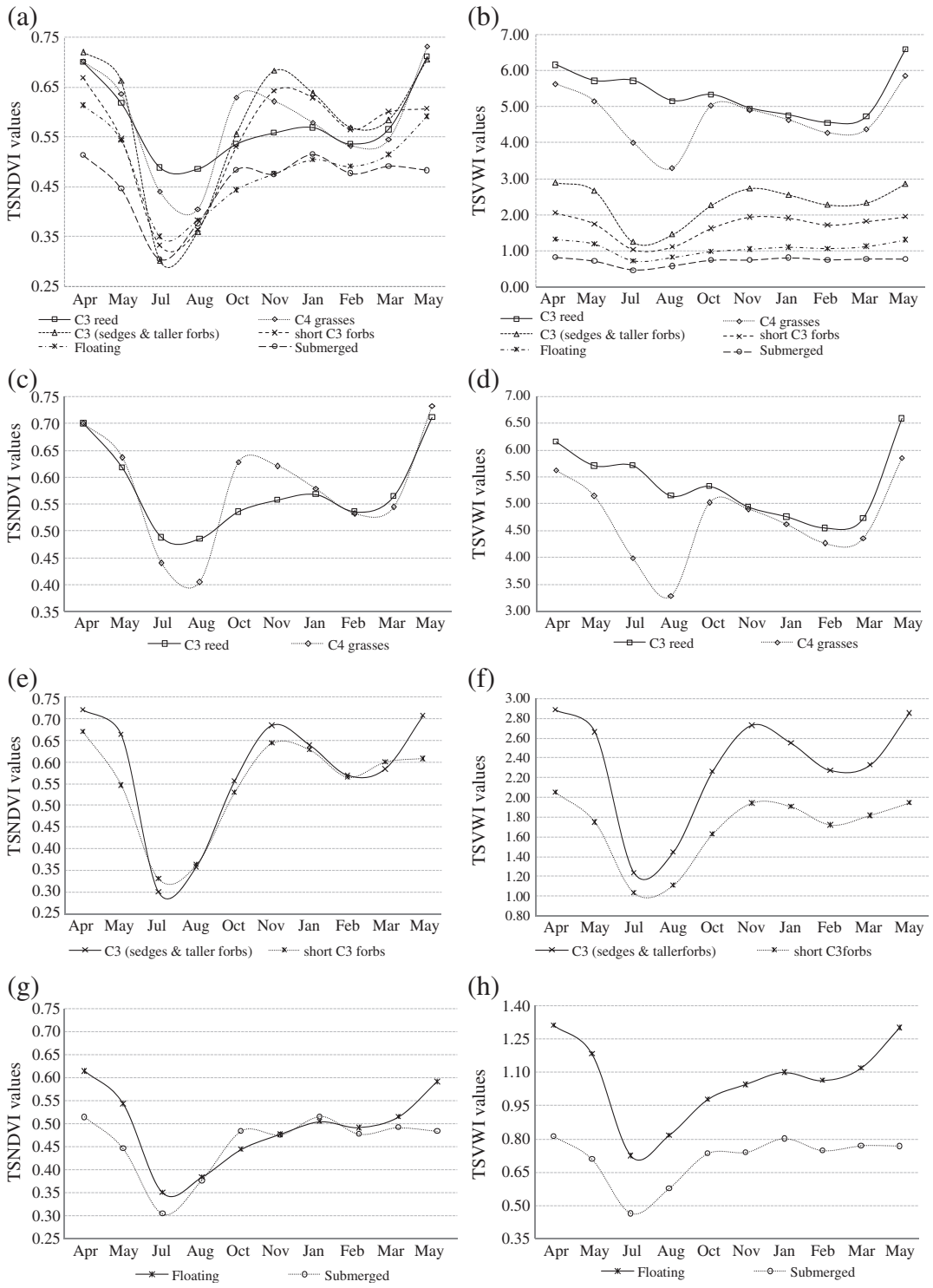

Fig. 5. Time-series NDVI curves and time-series VWI curves of different PFTs based on training samples from (a) time-series NDVI images and (b) time-series VWI images. (c) time-series NDVI images for C_4 grasses and C_3 reed, (d) time-series VWI images for C_4 grasses and C_3 reed, (e) time-series NDVI images for C_3 (sedges and taller forbs) and short C_3 forbs, (f) time-series VWI images for C_3 (sedges and taller forbs) and short C_3 forbs, (g) time-series NDVI images for floating and submerged aquatic macrophytes, (h) time-series VWI images for floating and submerged aquatic macrophytes. The training samples were selected at the image points corresponding to the field sample plots dominated by specific species with the highest homogeneity, the percent cover $\geq 80\%$, and the landscape composition homogeneity around the plots more than 60×60 m. The y-axis of Fig. 5(d), (f) and (h) were adjusted to the most appropriate range for each of two sub-groups in order to emphasize the effect of time-series VWI curves which obviously enhanced the separability between them.

VWI, respectively (Fig. 6). The overall accuracies of the three major PFTs classification were only 2.8% and 3.4% higher than those for the six minor PFTs for time series NDVI and time series VWI inputs, respectively. In turn, the overall accuracy of the time series VWI classification was 9.7% and 9.1% higher than that of time series NDVI for the three major and six minor PFT classifications, respectively (Fig. 6). These results indicated that the SVM algorithm with RBF was more sensitive to the information content of feature space than to the data dimensions.

Table 4
Pairwise comparisons of major and minor PFT classes using one-way ANOVA with Games–Howell post hoc test.

Class pair	Time-series NDVI differences across all dates		Time-series VWI differences across all dates	
	df	p-value	df	p-value
Major PFTs				
Emergent vs. hygrophilous	1594.90	0.49	1197.16	<0.001
Emergent vs. aquatic		<0.001		<0.001
Hygrophilous vs. aquatic		<0.001		<0.001
Minor PFTs				
The pairs of fall into one major class				
C_3 reed vs. C_4 grasses	1162.28	1.00	1060.22	0.33
C_3 (sedges and taller forbs) vs. short C_3 forbs		0.01		<0.001
Floating vs. submerged		<0.001		<0.001
The pairs of PFTs that may be spatial neighbors				
C_3 (sedges and taller forbs) vs. C_4 grasses	1162.28	0.97	1060.22	<0.001
C_3 (sedges and taller forbs) vs. C_3 reed		0.98		<0.001
short C_3 forbs vs. C_4 grasses		0.16		<0.001
short C_3 forbs vs. C_3 reed		0.10		<0.001

Note: we used the Welch statistic in Degrees of freedom (*df*) acquisition since it is more powerful than the standard F or Brown–Forsythe statistics when sample sizes and variances are unequal(Norušis, 2008). The quantity of samples was same as the number of training samples for each class.

In the final classification of the three major PFTs, hygrophilous vegetation was the most extensive class that occupied 26.3% (time series VWI-based) and 22.6% (time series NDVI-based) of the wetland area during Apr 2007–May 2008 (Fig. 7a, b). The time series VWI-based SVM classifier had a higher capacity for detecting short C_3 forbs with a producer's accuracy of 90.2% than the time series NDVI-based SVM classifier at 70.7% (Table 5, Fig. 7f). The area of aquatic macrophytes, the second largest major PFT, occupied 22.1% of the wetland area in the time series VWI-based classification map and 19.4% in the time series NDVI-based classification map (Fig. 7a, b). Within this major PFT, the producer's accuracy values for minor submerged aquatic macrophyte subclass were close between time series VWI (79.6%) and time series NDVI (77.4%). However, the accuracy of the second subclass, floating aquatic macrophytes, improved by 20.9% with time series VWI input (Fig. 7f), although this minor PFT was consistently the smallest, occupying only 3.7% (time series VWI-based) and 1.8% (time series NDVI-based) of the wetland area (Fig. 7c, d). Within the emergent plants (the smallest-area major PFT), the mapped extent of the C_3 reed subclass exceeded the area of C_4 grasses with time series NDVI as classification input (6.2% to 5.1%, respectively); however, it was lower than C_4 grass area with the time series VWI input (3.4% to 6.1%) (Fig. 7c, d).

Of the three non-vegetated cover types, sand occupied the smallest area by 1.3% (time series VWI-based) and 5.4% (time series NDVI-based) of the entire wetland (Fig. 7c, d, e). Both visual and quantitative examination of classification maps and images revealed that the spectral characteristics of this cover type were similar with

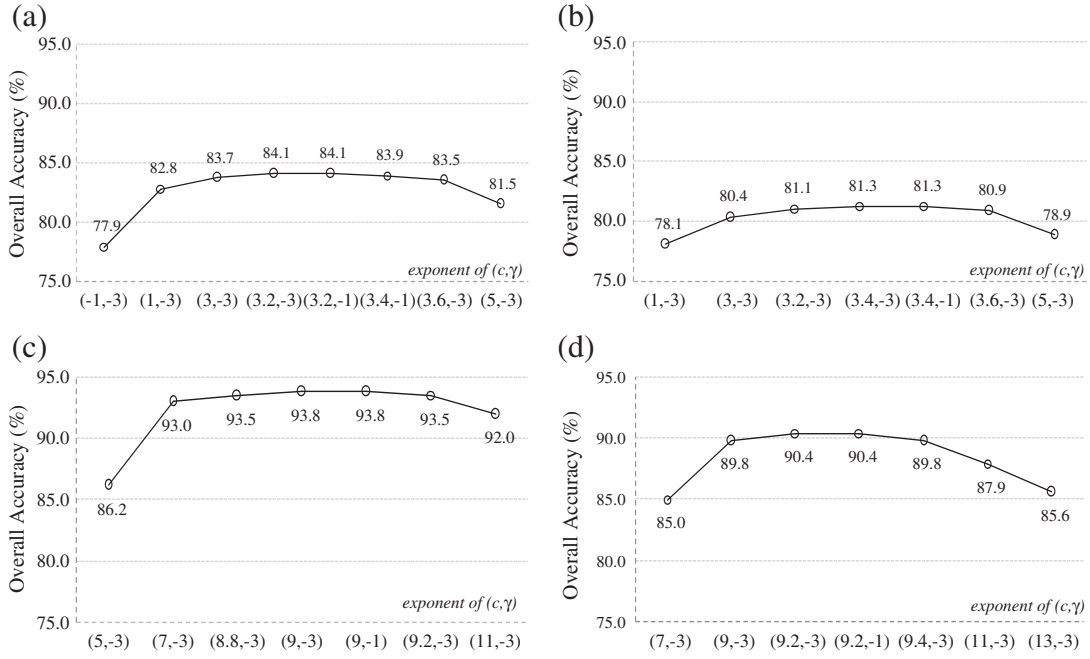

Fig. 6. The optimum pairs of parameter (*C*, γ) searching results for (a) time-series NDVI three general groups classification, (b) time-series NDVI six functional groups classification, (c) time-series VWI three general groups classification, and (d) time-series VWI six functional groups classification.

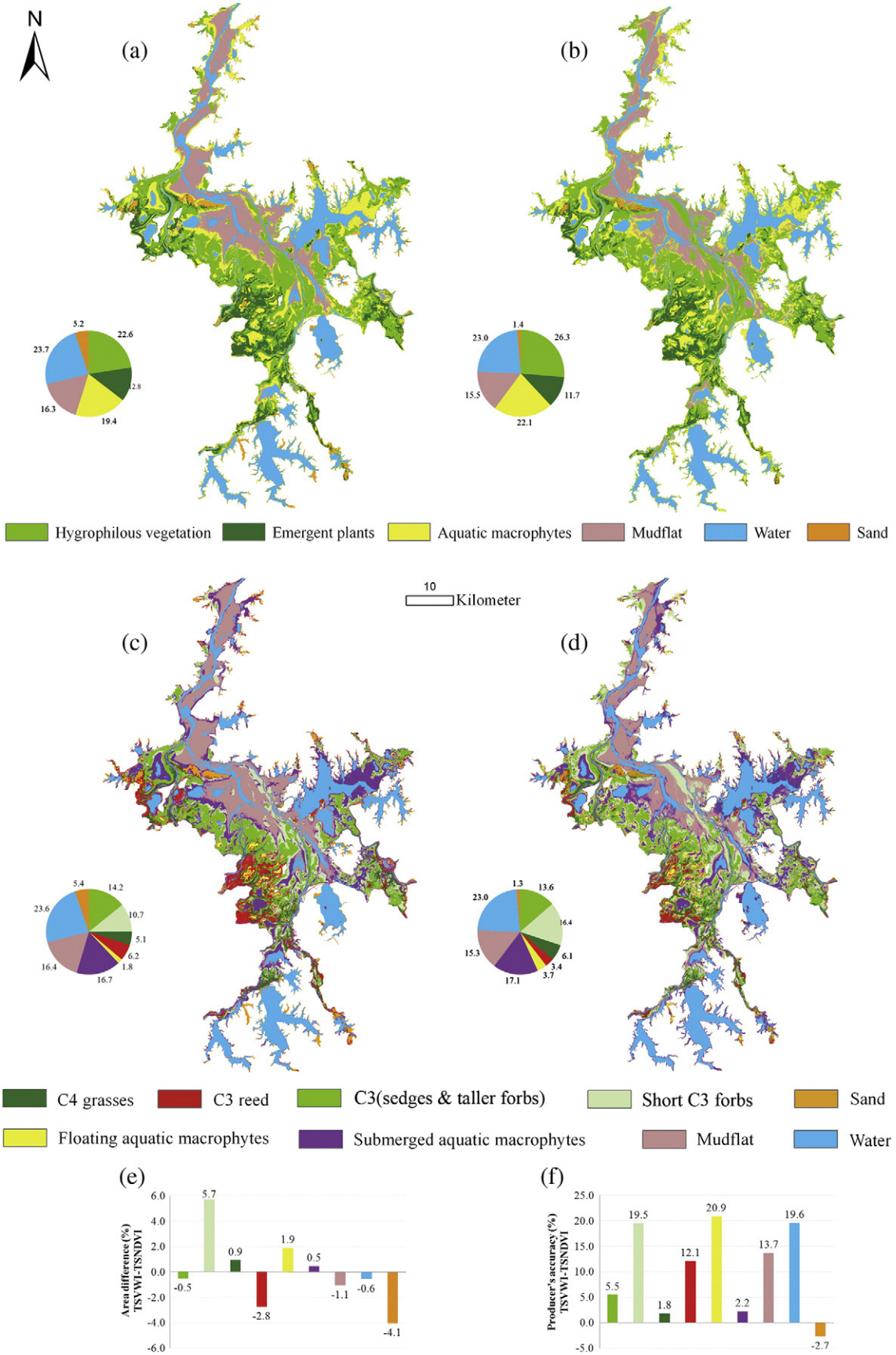

Fig. 7. Three major PFTs and six minor PFTs classification map using time-series NDVI and time-series VWI corresponding to the best pairs of (C, γ) respectively. (a) three major PFTs with time-series NDVI, (b) three major PFTs with time-series VWI, (c) six minor PFTs with time-series NDVI, and (d) six minor PFTs with time-series VWI images, (e) The area difference of each of functional groups occupied in time-series VWI-based and time-series NDVI-based classification results, (f) The Producer's accuracy difference of each of functional groups in time-series VWI-based and time-series NDVI-based classification results.

Table 5
Confusion matrix from time-series NDVI-based and time-series VWI-based classification for six functional groups, mudflat, water and sand, trained with 540 test samples. Prod. Acc. and User. Acc. stand for the Producer's Accuracy and the User's Accuracy. The right bottom corner of each classification is overall accuracy with Kappa in parentheses. Kappa is a statistical measure of inter-rater agreement for qualitative (categorical) items. The numbers in bold represent the number of correctly classified samples for each corresponding class.

	Ground truth (Pixels)										
Class	C_3 (sedges and taller forbs)	Short C_3 forbs	C_4 grasses	C_3 reed	Floating	Submerged	Mudflat	Water	Sand	Total	User. Acc. and Kappa
Time-series NDVI-based classification											
C_3 (sedges and taller forbs)	**66**	1	6	0	0	0	0	0	0	73	**90.4**
Short C_3 forbs	5	**29**	0	0	0	0	0	0	0	34	**85.3**
C_4 grasses	0	2	**48**	0	3	0	0	0	0	53	**90.5**
C_3 reed	1	1	1	**25**	9	2	0	0	0	39	**64.1**
Floating	0	0	0	0	**44**	2	0	2	0	48	**91.7**
Submerged	0	8	0	1	6	**72**	8	7	0	102	**70.6**
Mudflat	0	0	0	0	0	8	**36**	7	0	51	**70.6**
Water	0	0	0	0	0	2	0	**45**	0	47	**95.7**
Sand	0	0	0	7	5	7	0	0	**74**	93	**79.6**
Total	72	41	55	33	67	93	44	61	74	540	
Prod. Acc.	**91.7**	**70.7**	**87.3**	**75.8**	**65.7**	**77.4**	**81.8**	**73.8**	**100.0**		**81.3 (0.79)**
Time-series VWI-based classification											
C_3 (sedges and taller forbs)	**70**	2	6	2	0	0	0	0	0	80	**87.5**
Short C_3 forbs	2	**37**	0	0	2	0	0	0	2	43	**86.1**
C_4 grasses	0	0	**49**	2	0	0	0	0	0	51	**96.1**
C_3 reed	0	0	0	**29**	0	0	0	0	0	29	**100.0**
Floating	0	1	0	0	**58**	2	0	0	0	61	**95.1**
Submerged	0	1	0	0	7	**74**	2	4	0	88	**84.1**
Mudflat	0	0	0	0	0	7	**42**	0	0	49	**85.7**
Water	0	0	0	0	0	10	0	**57**	0	67	**85.1**
Sand	0	0	0	0	0	0	0	0	**72**	72	**100.0**
Total	72	41	55	33	67	93	44	61	74	540	
Prod. Acc.	**97.2**	**90.2**	**89.1**	**87.9**	**86.6**	**79.6**	**95.5**	**93.4**	**97.3**		**90.4 (0.89)**

C_3 reed class, and in some locations also with floating and submerged aquatic macrophytes, especially in winter when these three PFTs were senescent. However, since the submersion times of sand and PFTs were considerably different, the time series VWI-based classification largely corrected this confusion, which improved the user's accuracy for this class to 100% compared to 79.6% with time series NDVI (Table 5).

4. Discussion

4.1. The benefits of combining the traditional ecological PFT classification approaches with remote sensing analysis

Traditional ecological classifications of plant cover using ground surveys of vegetation often require considerable field sampling effort and time, even though they allow collecting very detailed information about plant and surface characteristics (examples are given in Tables 2 and 3). These efforts may be especially challenging in vast lake–wetland systems like Poyang Lake due to limited field access and risk of infectious disease (Hu et al., 2010; Marie et al., 2010; Niu et al., 2009). Alternatively, remotely sensed data can provide useful information on spectral characteristics and phenology of vegetation as well as landscape features which mediate the effects of flooding and other disturbances. Such information is important for detecting landscape patterns of vegetation distribution and their temporal variation, but in wetlands it is often difficult to obtain in situ. However, depending on the research objectives and required detail of plant classification, medium-resolution remote sensing imagery like the 32-m Beijing-1 data may be too coarse for accurate discrimination of the fine-scale vegetation types in heterogeneous wetland areas.

Our study has demonstrated the benefits of combining the traditional ecological PFT classification and remote sensing approach for a more comprehensive understanding of plant functional attributes of the Poyang Lake wetlands. Results raise several important questions for future discussion in the research community: Is a more detailed PFT classification scheme (i.e. including a large number of species and traits) likely to be more accurate than a simple scheme (i.e. only considering the dominant species and 1–2 key traits) when classes are delineated from remotely sensed data? To what extent can a remote sensing approach accurately describe spatial distribution of PFTs? When should we rely on detailed classification schemes to aid remote sensing classification? On the one hand, inclusion of more species and detailed traits into PFT classification schemes allows for more specific class definitions that can emphasize even minor constituents of plant cover. On the other hand, pixel-level reflectance data from satellite and airborne observations constrain detection to the dominant species in the canopy overstory, and thus characterize PFTs based on the most abundant ecosystem components (Graetz, 1990; Ustin & Gamon, 2010). For example, our field surveys included the 1×1 m plots with $\geq$80% cover by the short C_4 grass species *Cynodon dactylon* and *Paspalum distichum*; however, at the 32-m pixel level these species appeared more often as mixtures with tall C_4 grasses such as *Miscanthus sacchariflorus* and *M. floridulus* or C_3 (sedges and taller forbs). Therefore, our time series NDVI/VWI curves and final classification results primarily reflect the contributions from dominant overstory species of each PFT.

Nevertheless, several important conclusions can be tentatively made from our results. First, a detailed PFT classification scheme would likely require high-resolution remote sensing data to capture fine-scale vegetation mosaics, whereas a simple classification scheme based on dominant vegetation may be successful for representing broad-scale PFTs with medium-resolution imagery. Second, to accurately represent PFTs with less temporally stable distributions along inundation gradients such as in our study area, more frequent remotely sensed data and more detailed species information may be needed. Future research may extend our methods to adapt PFT classifications for more specific research objectives such as modeling landscape-level net primary productivity or carbon storage in vegetation components and improve reliability of PFT analysis from remotely sensed data. It may also be beneficial to develop novel remote sensing indices with higher sensitivity to vegetation diversity to capture the spatial and temporal

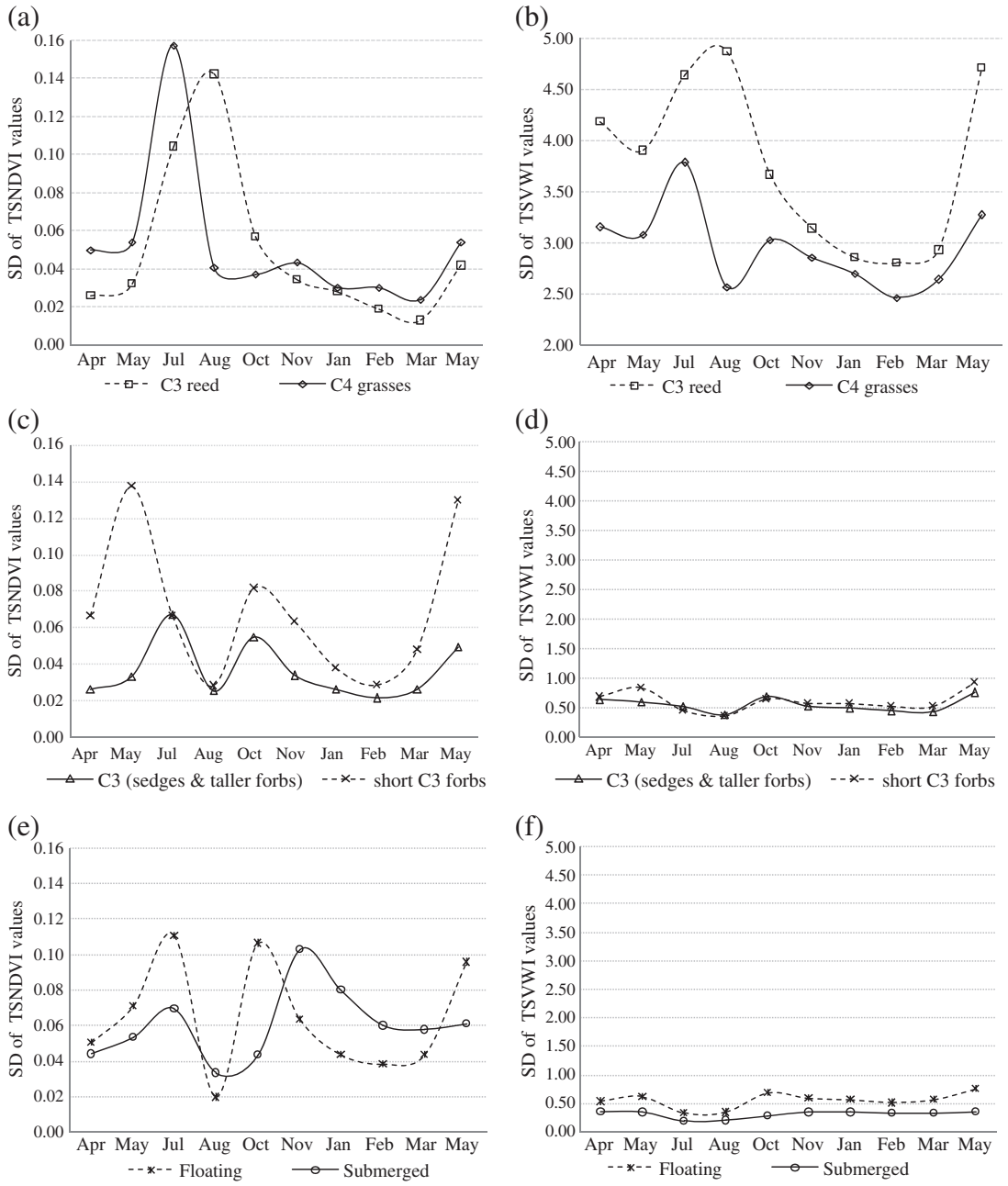

Fig. 8. The standard deviation (SD) of time-series NDVI curves and time-series VWI curves for (a) C_4 grasses and C_3 reed from time-series NDVI images, (b) C_4 grasses and C_3 reed from time-series VWI images, (c) C_3 (sedges and taller forbs) and short C_3 forbs from time-series NDVI images, (d) C_3 (sedges and taller forbs) and short C_3 forbs from time-series VWI images, (e) floating and submerged aquatic macrophytes from time-series NDVI images, and (f) floating and submerged aquatic macrophytes from time-series VWI images.

interactions between PFTs and their environmental controls and to facilitate integration of ground-based ecological information with time series of remotely sensed data across multiple spatial scales.

4.2. The uncertainty of time series NDVI and time series VWI curves

Considering relatively high diversity of species within each PFT class (e.g. 17 species in short C_3 forbs group, at least 6 species in C_4 grasses and C_3 reed groups), it is important to discuss the uncertainty in time series NDVI and time series VWI curves (Fig. 8) in order to assess the relative stability of phenological trends for each PFT and to analyze the sources of error in SVM classification.

Temporal patterns of standard deviations within PFT groups suggested that C_3 (sedges and taller forbs) exhibited the least phenological variation than other types at most image dates (Fig. 8c and d), and its producer's accuracy was relatively high with both time series NDVI (91.7%) and time series VWI (97.2%, Table 5), possibly but not exclusively for the following reasons. First, it was extensively dominated by Carex spp. (often ≥90% cover with minor accompanying forbs). Second, this type often formed vast homogeneous patches of more than 1×1 km around the sample plots in relatively flat areas with similar inundation start and end times. Finally, most areas of this type were not affected by low-magnitude water level fluctuations in winter according to field observations.

The most compositionally diverse PFT, short C_3 forbs, had higher SD values than C_3 (sedges and taller forbs), although change characteristics were largely consistent between these two PFTs (Fig. 8c and d). On the one hand, representative short C_3 forb areas with high abundance of *Potentilla limprichtii*, *Cardamine lyrate*, *Lapsana apogonoides* are usually adjacent to C_3 (sedges and taller forbs) areas in higher-elevation wetland locations. On the other hand, short C_3 forb patches with higher dominance of *Polygonum criopolitanum* and *P. hydropiper* often form a plaquelike landscape in narrow transitional zone between hygrophilous vegetation and aquatic macrophytes. These latter areas may be more strongly affected by low water level fluctuations in winter, which may cause the confusion of short C_3 forbs with floating or submerged aquatic macrophytes. Hence, these short C_3 forb areas may be particularly prone to disturbance from changing water levels and competitive pressure from either C_3 (sedges and taller forbs) if water table is declining, or from aquatic vegetation if water levels are increasing. These pressures may affect temporal stability of the short C_3 forbs distribution and their observed confusion with direct spatial neighbors (C_3 (sedges and taller forbs), floating and submerged macrophytes) in the time series VWI-based result (Table 5).

The C_3 reed group, though composed of only 6 species, exhibited more variability compared to other groups (Fig. 8a and b). Perennial C_3 reeds usually appear as stands either exclusively dominated by *Phragmites australis* along river banks, or mixed with some *Zizania caduciflora*, *Phalaris arundinacea*, *Heleocharis valleculosa* and *Juncus effusus* at lowland catchments. A large area of artificial *Phragmites australis* was planted in south of the Nanji Mountain river bank zone after 2004, which form highly homogeneous stands with the average annual submersion time of 1–2 months (July to August), whereas other species grow at various elevations with 2–4 months of average submersion time. Flood adaptation and relatively wide inundation tolerance of the dominant species could explain why this PFT had the second largest difference in percentage of PFT area between the time series VWI-based and time series NDVI-based classification results (2.8%, Fig. 7e). At the same time, in some locations this class may be confused with C_3 (sedges and taller forbs) since the dominant C_3 reed species (e.g., *H. valleculosa* and *P. arundinacea*) resemble some C_3 grasses by life form, height and photosynthetic pathway (Table 5).

In both classification outputs there was some misclassification of C_4 grasses with C_3 (sedges and taller forbs), although the curves between these two PFTs had significant difference in time series VWI curves (Table 4). This result was consistent with our field observations. Not only tall C_4 grasses such as *Miscanthus sacchariflorus* and *M. floridulus*, but also short C_4 grasses such as *Eremochloa ophiuroides* and *Paspalum distichum* were distributed along the narrow river banks of higher elevation. During low water level periods, these short C_4 grasses may be confused with C_3 (sedges and taller forbs) due to their frequent co-occurrence in transitional zones resulting in spectral mixtures of these two PFTs at the pixel level. At the same time, harvesting of taller C_4 grasses and burning of these sites by local people together with cooler winter weather conditions potentially favoring C_3 species may result in temporary colonization of C_4 sites by spreading C_3 (sedges and taller forbs).

The two aquatic PFTs were typically found at lower elevation zones with more than 6 months of annual submersion time. They were strongly affected by changes in the water table, especially during water infilling and recession periods (Fig. 8e and f). On the one hand, some species of submerged aquatic macrophytes (e.g. *Potamogeton crispus* and *Limnophila sessiliflora*) grow in the winter period, and may be more sensitive to low water level fluctuation than floating-leaved vegetation from Nov. to March (Fig. 8e). On the other hand, submerged aquatic macrophytes group may occasionally be misclassified with either floating or mudflat and water (2, 7, 10 confusion sample points for each of pairs from time series VWI classification, Table 5) since they were naturally co-occurring spatial neighbors. Furthermore, some floating aquatic species may be amphibious supporting biomass both above and below water and, therefore, may be hard to distinguish at the 32-m pixel level. Specifically, sporadic local increases in water turbidity which may occur due to sediment movement and human activities such as sand dredging (Wu, 2008) may obscure submerged vegetation in locations where it is present. This, together with the effect of the water layer on reflectance from submerged vegetation, may lead to underestimation of this PFT in our classification results.

4.3. Time series NDVI-based vs. time series VWI-based classification

Time series NDVI was useful for separating different PFTs and also was likely sensitive to phenological and ecophysiological characteristics affecting spectral signatures of the three major PFTs within a year. However, the hierarchical relationship between six minor PFTs and their more general groups distinguished by inundation tolerance (emergent plants, hygrophilous vegetation and aquatic macrophytes; Fig. 4) was not obvious from the NDVI curves (Fig. 5a). In contrast, time series VWI, which combined time series NDVI images and the submersion time index, more effectively separated the six minor PFTs according to their respective major PFTs (Fig. 5b, Table 4). Furthermore, time series VWI better emphasized the contrasts between the pairs of PFTs that may be spatial neighbors (Table 4). The SVM classification of the time series VWI images improved classification accuracy relative to time series NDVI input for most classes, but the greatest improvement occurred with PFTs sensitive to water table changes—floating aquatic macrophytes and short C_3 forbs, from 65.7% to 86.6% and 70.7% to 90.2%; and with the PFT that had wider adaptation to water table conditions—C_3 reed, from 75.8% to 87.9%, respectively (Table 5, Fig. 7f). Classification accuracies indicated that in general, time series NDVI could be potentially useful in mapping aquatic PFTs with an overall accuracy of 81.3% and Kappa value of 0.79. However, by combining the information on the water fluctuation characteristics (submersion time) with the time series NDVI-based greenness, the time series VWI could better discern different aquatic PFTs and yielded more accurate results with an overall accuracy of 90.4% and Kappa value of 0.89.

These results have important implications for the analysis of seasonal dynamics of wetland surface. From a remote sensing standpoint phenological changes in vegetation may affect detection of the water body in the imagery: senescence of emergent and floating species in the fall may expose new open water areas or water containing submerged vegetation, which does not necessarily indicate expansion of the existing water table (Dronova et al., 2011). In contrast, inundation of the mudflats by the first spring rains may produce local increases in the extent of the water body. While at Poyang Lake the monsoon rain season strongly affects expansion and recession of the water table, local hydrological variation at different parts of this wetland is likely driven by a complex array of factors which are still not well understood (Andreoli et al., 2007; Min, 2004; Shankman et al., 2006). These drivers include hydrological variation in the river discharge, regulation of water levels by local dams, the effect of sediment movement and bank erosion on the depth of pools and river beds and transpiration of the dense stands of emergent aquatic vegetation. These processes, in turn, affect the submersion time index and time series VWI calculation and thus the accuracy of characterizing functional diversity of wetland vegetation and its change. Thus, future research will benefit from incorporating more accurate algorithms for characterization of wetland inundation cycle (Feng et al., 2011; Hui et al., 2008; Zhao et al., 2011) and more detailed and accurate bathymetry and fine-scale elevation data into PFT analysis. Another promising strategy is using novel sensors and fusion of multiple data sources, for instance, combining sonar measurements and high spatial resolution synthetic aperture radar (SAR) imagery (Hess et al., 2003; Kasischke et al., 2003; Shen et al., 2008; Wang et al., 2012), utilizing RADAR and LIDAR technologies to obtain vegetation structure (Huang et al., 2011) and combining RADAR/LIDAR with visible-infrared sensors for mapping dominant PFTs and characterizing their biomass and canopy structure.

4.4. Other related research and future work

Given the high seasonal variability of Poyang Lake flood extents and surface composition (Dronova et al., 2011; Shankman et al., 2006; Wu, 2008), our classification was intended to represent PFTs that are prevalent for most of the year except the monsoonal flood season during June–August, while their exact boundaries may vary following the dynamics of the water body cover within a year. Thus, our analysis represents the first step in mapping "temporally" dominant PFTs from remotely sensed data in the context of the whole-year wetland dynamics. These mapped PFTs may provide a useful baseline for subsequent analyses of the inner-annual spatio-temporal variation in specific classes and for selection of priority target research sites and field sampling of PFTs in the future work. In addition, even the locations with potentially higher classification uncertainty such as mapped boundaries between PFT classes may represent "hotspot" regions for future studies of vegetation succession and specific dynamics of PFT distributions in this landscape (Zhao et al., 2009). Future work should extend our approaches to characterize the inner-annual spatio-temporal variation in PFTs, which may be used in landscape modeling of the changes in bird habitats, plant biogeochemical cycling and ecological productivity associated with different PFTs under different scenarios of water level fluctuations, climate change and human activities in this area. These assessments may eventually be combined with green house gas flux simulation models (Li, 2007; Li & Frolking, 1992; Mummey et al., 1998) for scaling up site-based or PFT-based observations to the whole Poyang Lake and middle Yangtze River basin regions.

5. Conclusions

The main purpose of this study was to better understand the seasonal dynamics of wetland surface composition, and to explore whether the microsatellite sensors combining multispectral, medium spatial resolution, large-area coverage and frequent revisit time would have the ability to successfully depict the spatial distribution of the vast wetland plant functional types. To achieve this objective, a PFT classification scheme was proposed based on a two-step hierarchical cluster analysis of 51 dominant wetland species by 10 ecological traits at the species level and 4 characteristics at the sample plot level. We then used a time series of Beijing-1 microsatellite data to classify those PFTs for the whole study area. To our knowledge, this is the first attempt to apply the most frequently acquired medium-resolution satellite data, Beijing-1 imagery, for plant type mapping over a large and relatively inaccessible wetland area like Poyang Lake. Our proposed methods could be applied to other wetland systems globally which undergo seasonal inundation due to hydrologic and climatic cycles. The success of PFT classification using SVM algorithm was improved by combining the multi-temporal index of vegetation greenness with the estimates of wetland submersion times based on the changes in the mapped water extent. The proposed time series VWI, a repeatable and easy-to-understand indicator of phenological–hydrological characteristics of PFTs, represented the association between the freshwater aquatic PFT distribution and water fluctuations at the regional scale, and thus improved the classification accuracy, especially for PFT classes that were particularly sensitive or had wider adaptation to water level fluctuation. Our results and maps could be used as the baseline for future research on plant functional pattern variation for the whole Poyang Lake ecosystem, as well as for ecological monitoring and assessment of potential impacts of anthropogenic pressures on this wetland.

Acknowledgments

This research is partially supported by the National Natural Science Foundation of China (grant no. 30590370) and Open Fund of State Key Laboratory of Remote Sensing Science (OFSLRSS201101) and a grant from the National High Technology Program of China (2009AA 12200101) and the Basic Research and Operating Program of Chinese Academy of Fishery Sciences (2012 C004). We also thank Prof. Wan Wenhao from Nanchang University,Jiangxi Province for his guidance during the vegetation field investigations and his suggestion for PFTs mapping, to Beijing Twenty-First Century Science and Technology Development Co, Ltd for supplying Beijing-1 satellite images for this research. Finally, we thank three anonymous reviewers for their time and useful feedback that helped to improve this paper.

References

Ackerly, D. D., & Cornwell, W. K. (2011). A trait-based approach to community assembly: partitioning of species trait values into within- and among-community components. *Ecology Letters*, *10*, 135–145.

Andreoli, R., Yésou, H., Li, J., & Desnos, Y. L. (2007). Synergy of low and medium resolution ENVISAT ASAR and optomal data for lake watershed monitoring: Case study of Poyang Lake (Jiangxi Province, P.R. of China). *Proceedings of 'ENVISAT Symposium2007', Montreux, Switzerland 23–27 April 2007(ESA SP-636, July 2007)*.

Barter, M., Chen, L. W., Cao, L., & Lei, G. (2004). Waterbird survey of the middle and lower Yangtze River floodplain in late January and early February 2004. *WWF China reports*. Beijing: China Forestry Publishing House.

Barter, M., Lei, G., & Cao, L. (2006). *Waterbird survey of the Middle and Lower Yangtze River Floodplain (February 2005)*. Beijing, China: World Wildlife Fund–China and Chinese Forestry Publishing House 64 pp.

Barzen, J. (2008). Phase 1 Report: How development projects may impact wintering waterbirds at Poyang Lake. Unpublished report submitted to hydro-ecology Institute of the Yangtze Water Resources Commission. International Crane Foundation, Baraboo, Wisconsin, USA. 14 pp.

Barzen, J., Engels, M., Burnham, J., Harris, J., & Wu, G. (2009). Phase 2 Report: Potential impacts of a water control structure on the abundance and distribution of wintering waterbirds at Poyang Lake. Unpublished report submitted to Hydroecology Institute of the Yangtze Water Resources Commission. International Crane Foundation, Baraboo. Wisconsin, USA. 54 pp.

Beale, C. V., Bint, D. A., & Long, S. P. (1996). Leaf photosynthesis in the C_4-grass Miscanthus×giganteus, growing in the cool temperate climate of southern England. *Journal of Experimental Botany*, *47*, 267–273.

Bonan, G. B., Levis, S., Kergoat, L., & Oleson, K. W. (2002). Landscapes as patches of plant functional types: An integrating concept for climate and ecosystem models. *Global Biogeochemical Cycles*, *16*, http://dx.doi.org/10.1029/2000GB001360.

Boutin, C., & Keddy, P. A. (1993). A functional classification of wetland plants. *Journal of Vegetation Science*, *4*, 591–600.

Cao, M. K., & Woodward, F. I. (1998). Dynamic responses of terrestrial ecosystem carbon cycling to global climate change. *Nature*, *393*, 249–252.

Chapin, F. S., III, Walker, B. H., Hobbs, R. J., Hooper, D. U., Lawton, J. H., Sala, O. E., et al. (1997). Biotic control over the functioning of ecosystems. *Science*, *277*, 500–504.

Cheng, T. H. (1987). *A synopsis of the avifauna of China.* Beijing: Science Press 1223 pp.

Cowardin, L. M., Carter, V., Golet, F. C., & LaRoe, E. T. (1979). *Classification of wetlands and deepwater habitats of the United States.* Washington, D.C. Jamestown, ND: Northern Prairie Wildlife Research Center: U. S. Department of the Interior, Fish and Wildlife Service 79 pp.

Díaz, S. (1995). Elevated-CO_2 responsiveness, interactions at the community level, and plant functional types. *Journal of Biogeography*, *22*, 289–295.

Díaz, S., & Cabido, M. (1997). Plant functional types and ecosystem function in relation to global change. *Journal of Vegetation Science*, *8*, 463–474.

Dronova, I., Gong, P., & Wang, L. (2011). Object-based analysis and change detection of major wetland cover types and their classification uncertainty during the low water period at Poyang Lake, China. *Remote Sensing of Environment*, *115*, 3220–3236.

Edwards, E. J., Osborne, C. P., Strömberg, C. A. E., Smith, S. A., & C4 Grasses Consortium (2010). The origins of C_4 grasslands: Integrating evolutionary and ecosystem science. *Science*, *328*, 587–591.

Epstein, H. E., Chapin, F. S., III, Walker, M. D., & Starfield, A. M. (2001). Analyzing the functional type concept in arctic plants using a dynamic vegetation model. *Oikos*, *95*, 239–252.

Fang, J. Y., Wang, Z. H., Zhao, S. Q., Li, Y. K., Tang, Z. Y., Yu, D., et al. (2006). Biodiversity changes in the lakes of the central Yangtze. *Frontiers in Ecology and the Environment*, *4*, 369–377.

Feng, L., Hu, C. M., Chen, X. L., Li, R. F., Tian, L. Q., & Murch, B. (2011). MODIS observations of the bottom topography and its inter-annual variability of Poyang Lake. *Remote Sensing of Environment*, *115*, 2729–2741.

Finlayson, M., Harris, J., McCartney, M., Young, L., & Chen, Z. (2010). *Report on Ramsar visit to Poyang Lake Ramsar site, P.R. China 12–17 April 2010.* Report prepared on behalf of the Secretariat of the Ramsar Convention 34 pp. http://www.ramsar.org/pdf/Poyang_lake_report_v8.pdf.

Foody, G. M., & Mathur, A. (2004). Toward intelligent training of supervised image classifications: Directing training data acquisition for SVM classification. *Remote Sensing of Environment*, *93*, 107–117.

Gong, P., Miller, J. R., & Spanner, M. (1994). Forest canopy closure from classification and spectral unmixing of scene component–multisensor evaluation of an open canopy. *IEEE Transactions on Geoscience and Remote Sensing*, *32*, 1067–1080.

Gong, P., Niu, Z. G., Cheng, X. A., Zhao, K. Y., Zhou, D. M., Guo, J. H., et al. (2010). China's wetland change (1990–2000) determined by remote sensing. *Science in China Series D: Earth Sciences*, *53*, 1036–1042.

Graetz, R. D. (1990). Remote sensing of terrestrial ecosystem structure: An ecologist's pragmatic view. In R. J. Hobbs, & H. A. Mooney (Eds.), *Remote Sensing of Biosphere Functioning* (pp. 5–30). Berlin: Springer-Verlag.

Hess, L. L., Melack, J. M., Novo, E. M. L. M., Barbosa, C. C. F., & Gastil, M. (2003). Dual-season mapping of wetland inundation and vegetation for the central Amazon basin. *Remote Sensing of Environment*, *87*, 404–428.

Hsu, C. C., Chang, C. C., & Lin, C. J. (2010). A practical guide to support vector classification. http://www.csie.ntu.edu.tw/~cjlin

Hu, H. T., Gong, P., & Xu, B. (2010). Spatially explicit agent-based modelling for schistosomiasis transmission: Human–environment interaction simulation and control strategy assessment. *Epidemics*, *2*, 49–65.

Huang, H. B., Li, Z., Gong, P., Cheng, X., Clinton, N., Cao, C. X., et al. (2011). Automated methods for measuring DBH and tree heights with a commercial scanning LiDAR. *Photogrammetric Engineering and Remote Sensing*, *77*, 219–227.

Hui, F. M., Xu, B., Huang, H. B., Yu, Q., & Gong, P. (2008). Modelling spatial–temporal change of Poyang Lake using multitemporal Landsat imagery. *International Journal of Remote Sensing*, *29*, 5767–5784.

Hutchinson, G. E. (1975). *A treatise on limnology. Vol III. Limnological botany*. New York, NY: Wiley 672 pp.

Ji, W. T., Zeng, N. J., Wang, Y. H., Gong, P., Xu, B., & Bao, S. M. (2007). Analysis on the waterbirds community survey of Poyang Lake in winter. *Geographic Information Sciences*, *13*, 51–64.

Johnston, R. M., & Barson, M. M. (1993). Remote sensing of Australian wetlands: An evaluation of Landsat TM data for inventory and classification. *Australian Journal of Marine & Freshwater Research*, *44*, 235–252.

Junk, W. J. (Ed.). (1997). *The Central Amazon Floodplain: Ecology of a pulsing system, ecological studies*. Berlin: Springer 126 pp.

Kasischke, E. S., Smith, K. B., Bourgeau-Chavez, L. L., Romanowicz, E. A., Brunzell, S., & Richardson, C. J. (2003). Effects of seasonal hydrologic patterns in south Florida wetlands on radar backscatter measured from ERS-2 SAR imagery. *Remote Sensing of Environment*, *88*, 423–441.

Kavzoglu, T., & Colkesen, I. (2009). A kernel functions analysis for support vector machines for land cover classification. *International Journal of Applied Earth Observation and Geoinformation*, *11*, 352–359.

Keddy, P. A. (1992). A pragmatic approach to functional ecology. *Functional Ecology*, *6*, 621–626.

Lenssen, J., Menting, F., Van Der Putten, W., & Blom, K. (1999). Control of plant species richness and zonation of functional groups along a freshwater flooding gradient. *Oikos*, *86*, 523–534.

Li, C. S. (2007). Quantifying greenhouse gas emissions from soils: Scientific basis and modeling approach. *Soil Science and Plant Nutrition*, *53*, 344–352.

Li, J. (2009). Scientists line up against dam that would alter protected wetlands. *Science*, *326*, 508–509.

Li, C. S., & Frolking, T. A. (1992). A model of nitrous oxide evolution from soil driven by rainfall events, I. Model structure and sensitivity. *Journal of Geophysical Research*, *97*, 9759–9776.

Li, R., & Liu, J. (2002). Wetland vegetation biomass estimation and mapping from Landsat ETM data: A case study of Poyang Lake. *Journal of Geographic Sciences*, *12*, 35–41.

Liu, X. Z., & Ye, J. X. (2000). *The Jiangxi Wetland*. Beijing, China: China Forest Publishing Company (in Chinese).

Marie, T., Lai, X., Huber, C., Chen, X., Uribe, C., Huang, S., et al. (2010). Monitoring temporal evolution of the presence intermediate host of the Schistosomiasis and its risk transmission based on DRAGON times series in Poyang Lake area, Jiangxi province, P.R. China. *ESA SP 686, Proceeding of «Living Planet Symposium », 27 June–2 July 2010, Bergen, Norway*.

Marion, L., & Paillison, J. M. (2003). A mass balance assessment of the contribution of floating-leaved macrophytes in nutrient stocks in an eutrophic macrophyte-dominated lake. *Aquatic Botany*, *75*, 249–260.

McGill, B. J., Enquist, B. J., Weiher, E., & Westoby, M. (2006). Rebuilding community ecology from functional traits. *Trends in Ecology & Evolution*, *21*, 178–185.

Melillo, J. M., McGuire, A. D., Kicklighter, D. W., Moore, B., Vorosmarty, C. J., & Schloss, A. (1993). Global climate change and terrestrial net primary production. *Nature*, *363*, 234–240.

Menges, E. S., & Waller, D. M. (1983). Plant strategies in relation to elevation and light in flood plain herbs. *The American Naturalist*, *122*, 454–473.

Michishita, R., Xu, B., & Gong, P. (2008). A decision tree classifier for the monitoring of wetland vegetation using ASTER data in the Poyang Lake region, China. The International Archives of the Photogrammetry. *Remote Sensing and Spatial Information Sciences*, *37B8*, 315–321.

Min, Q. (2004). Analysis and calculation of frequency variation of flood stages in Poyang Lake. *Hydrology*, *24*, 17–20.

Mummey, D. L., Smith, J. L., & Bluhm, G. (1998). Assessment of alternative management practices on N_2O emissions from US agriculture. *Agriculture, Ecosystems & Environment*, *70*, 79–87.

Niu, Z. G., Gong, P., Cheng, X., Guo, J. H., Wang, L., Huang, H. B., et al. (2009). Geographical characteristics of China's wetlands derived from remotely sensed data. *Science in China Series D: Earth Sciences*, *52*, 723–738.

Niu, Z. G., Zhang, H. Y., & Gong, P. (2011). More protection for China's wetlands. *Nature*, *471*, 305.

Norušis, M. J. (2008). *IBM SPSS Statistics 19 guide to data analysis*. New Jersey: Prentice Hall Press 672 pp.

Peñuelas, J., Gamon, J. A., Griffin, K., & Field, C. B. (1993). Assessing community type, plant biomass, pigment composition, and photosynthetic efficiency of aquatic vegetation from spectral reflectance. *Remote Sensing of Environment*, *46*, 1–25.

Poorter, H. (1993). Interspecific variation in the growth response of plants to an elevated ambient CO_2 concentration. *Plant Ecology*, *104–105*, 77–97.

Qi, S. H., Brown, D. G., Tian, Q., Jiang, L. G., Zhao, T. T., & Bergen, K. M. (2009). Inundation extent and flood frequency mapping using Landsat imagery and digital elevation models. *GIScience and Remote Sensing*, *46*, 101–127.

Shankman, D., Keim, B., & Song, J. (2006). Flood frequency in China's Poyang Lake region: Trends and teleconnections. *International Journal of Climatology*, *26*, 1255–1266.

Shen, G. Z., Guo, H. D., & Liao, J. J. (2008). Object oriented method for detection of inundation extent using multi-polarized synthetic aperture radar image. *Journal of Applied Remote Sensing*, *2*, 023512.

Smith, T. M., Shugart, H. H., & Woodward, F. I. (Eds.). (1997). *Plant functional types: Their relevance to ecosystem properties and global change*. New York: Cambridge University Press 369 pp.

Still, C. J., Berry, J. A., Collotz, G. J., & DeFries, R. S. (2003). Global distribution of C_3 and C_4 vegetation: Carbon cycle implications. *Global Biogeochemical Cycles*, *17*, 1006–1020.

Strahler, A., Muchoney, D., Borak, J., Friedl, M., Gopal, S., Lambin, E., et al. (1999). *MODIS land cover product algorithm theoretical basis document*. Boston, MA: Boston University Version 5.0.

Sun, W. X., Liang, S. L., Xu, G., Fang, H. L., & Dickinson, R. (2008). Mapping plant functional types from MODIS data using multisource evidential reasoning. *Remote Sensing of Environment*, *112*, 1010–1024.

Tax, D. M. J., & Duin, R. P. W. (2004). Support vector data description. *Machine Learning*, *54*, 45–66.

Ustin, S. L., & Gamon, J. A. (2010). Remote sensing of plant functional types. *The New Phytologist*, *186*, 795–816.

Wang, X. H. (2004). *Poyang lake ecosystem assessment*. Beijing: Science Press 218 pp.

Wang, X. W., Cheng, X., Li, Z., Huang, H. B., Niu, Z. G., Li, X. W., et al. (2012). Lake water footprints identification from time-series ICESat/GLAS data. *IEEE Geoscience and Remote Sensing Letters*, *9*, 333–337.

Warner, B. G., & Rubec, C. D. A. (1997). *The Canadian Wetland Classification System* National Wetlands Working Group, Ontario, Waterloo (second ed.): University of Waterloo, Wetlands Research Centre 76 pp.

Wilksinson, L. (1984). *SYSTAT*. Evanston, II: The system for statistics. Systat Inc.

Wright, C., & Gallant, A. (2007). Improved wetland remote sensing in Yellowstone National Park using classification trees to combine TM imagery and ancillary environmental data. *Remote Sensing of Environment*, *107*, 582–605.

Wu, G. (2008). Impact of human activities on water level and clarity and underwater light climate of Vallisneria spiralis L. in Poyang Lake, China. Wageningen University 2008. ITIC Dissertation. 117 pp.

Zhang, B. (Ed.). (1988). *Study on Poyang Lake*. Shanghai: Shanghai Publishing House of Science and Technology (in Chinese).

Zhao, X., Stein, A., & Chen, X. L. (2011). Monitoring the dynamics of wetland inundation by random sets on multi-temporal images. *Remote Sensing of Environment*, *115*, 2390–2401.

Zhao, B., Yan, Y., Guo, H. Q., He, M. M., Gu, Y. J., & Li, B. (2009). Monitoring rapid vegetation succession in estuarine wetland using time series MODIS-based indicators: An application in the Yangtze River Delta area. *Ecological Indicators*, *9*, 346–356.

Zheng, Y. (2009). Prediction of the distribution of C_3 and C_4 plant species from a GIS-based model: A case study in Poyang Lake, China. MSc thesis, ITC, Enschede, the Netherlands.

Zheng, Y. M., Zhang, H. Y., Niu, Z. G., & Gong, P. (2012). Preliminary assessment of protection effectiveness of national wetland natural reserves in China. *Chinese Science Bulletin*, *57*, 1116–1134.